Effectiveness of water-oriented thinning in two semiarid forests: the redistribution of increased net rainfall into soil water, drainage and runoff

Antonio D. del Campo[1*], María González-Sanchis[1], Antonio J. Molina[2], Alberto García-Prats[1], Carlos J. Ceacero[3], Inmaculada Bautista[1]

[1]Research Group in Forest Science and Technology (Re-ForeST), Research Institute of Water and Environmental Engineering (IIAMA), Universitat Politècnica de València, Camino de Vera s/n, E-46022 Valencia (Spain)

[2]Surface Hydrology and Erosion Group, Institute of Environmental Assessment and Water Research (IDAEA-CSIC), Jordi Girona 18-26, E-08034 Barcelona (Spain)

[3]Departamento de Fisiología, Anatomía y Biología celular, Universidad Pablo de Olavide, E-41013, Sevilla (Spain)

[*]Corresponding author: ancamga@upv.es

Phone: 0034963877966

Fax: 0034963877618

Key words: adaptive silviculture, forest hydrology, Aleppo pine *Pinus halepensis*, Holm oak *Quercus ilex*, boosted regression trees, elasticity analysis.

Abstract

Water is the key element that modulates the provision of goods and services together with global/climate stressors affecting semiarid forests. In this sense, there is a need to improve the understanding and quantification of forest and water relationships as affected by forest management. This work addresses this issue by comparing net rainfall (Pn) redistribution into different belowground hydrological processes (BHP) in two forest types after a thinning treatment: a holm oak coppice (HU) and a post-fire Aleppo pine regeneration (CAL). The relative contribution (RI) of forest structure, antecedent soil moisture (θ_{st}), rainfall and meteorological conditions on the BHP was assessed through boosted regression trees models. In both sites, the RI of the forest structure itself was limited (<10%). However, θ_{st}, which clearly increased significantly with thinning, received an average RI of 29%. Surface and subsurface lateral flows showed values <1% of gross rainfall (Pg) in either site and were not significantly affected by thinning. On the other hand, soil moisture and drainage were affected by the thinning treatment, although with different extent depending on the site: in the drier site (CAL), the increased Pn in the thinning was mainly allocated into increased soil water content, with very limited improvement in drainage (<10 mm/year); in contrast, in the wetter continental site of HU, drainage to deeper soil layers was the most remarkable effect of thinning (50 mm/year higher than in control), given the higher θ_{st} and hence the lower soil water storage available. Thinning also improved the response of BHP during drought, making these processes more elastic and less vulnerable to climatic extremes. The results presented here complement those previously reported on rainfall partitioning in these sites and all together provide a comprehensive understanding of the short-term effect (3-4 years) of water-oriented silviculture *Quercus ilex* and *Pinus halepensis* low-biomass semiarid

forests. Questions such as the long-term effects of thinning remain open for these ecosystems.

1. Introduction

Forests affect all components of the water cycle from global to local scales (Ellison et al., 2017), which has prompted for different water-oriented management strategies along the last decades (Hibbert et al., 1982, Sahin and Hall, 1996; Troendle et al., 2001; Ganatsios et al., 2010). More recently, the focus of these strategies has been put on increasing soil water and aquifer recharge rather than increasing runoff and/or streamflow (Creedy and Wurzbacher, 2001; Grant et al., 2013; Ungar et al., 2013; Klein et al., 2013; del Campo et al., 2014; Ilstedt et al., 2016). This is an eco-hydrological approach that considers improving forest resilience through a watering effect on the trees remaining after silvicultural intervention, and it has emerged especially for semiarid forests where the provision of goods and services is threatened by global changes and the related more intense droughts (Allen et al., 2010; Lindner et al., 2014). In any case, water is the key element that modulates either the provision of goods and services or the global and climate stressors affecting semiarid forests, such as increased risk of fire (Hurteau et al., 2008; García-Prats et al., 2015), blue/green water impairment (Grant et al., 2013; González-Sanchis et al., 2015), growth stagnation, higher tree-climate sensitivity, drought stress and mortality (López et al., 2009; García de la Serrana et al., 2015; Fernandes et al., 2016). In the context of *difficult* hydrology (Grey and Sadoff, 2007) characterized by water scarcity, marked seasonality with torrential events followed by long dry seasons, combination of high intra and inter-annual variability, etc., water-oriented forest management should necessarily pay especial attention to both soil water storage and

groundwater recharge (Ilstedt et al., 2016; García-Prats et al., 2016), given their key roles in maintaining watershed and ecosystem resilience.

In the topic of forest-water relationships and their affection through forest management, the belowground hydrological processes (BHP) have received little attention as compared to the aboveground processes, in spite of the role that forest structure (above and belowground) plays on the dynamics of soil hydrology (Devitt and Smith, 2002; Lin and Zhou, 2008; Coenders-Gerrit, 2012; Bachmair et al., 2012). The manipulation of vegetation has a primary impact on net precipitation at the short term, as increased throughfall and stemflow may enhance soil moisture and the related flows (Taniguchi et al., 1996; Liang et al., 2011; Molina et al., 2019). Thereafter, when biomass is removed, the net rainfall partitioned into soil water replenishment and vertical water flow may locally change, thus affecting lateral water flow (Dung et al., 2012). However, this simple conceptualization becomes more complex in the reality, as the horizontal and vertical heterogeneity of the soil properties in forested hillslopes make predicting soil water content difficult, but also the soil water flows given that the macropores created by plant roots and burrowing animals can be laterally and/or vertically connected over several meters (Lin and Zhou, 2008; Beven and Germann, 2013). In addition, other factors such as antecedent soil moisture, rainfall characteristics, meteorology during rainfall, topography and slope length also play fundamental roles in explaining soil hydrology variability for a particular forest (Gómez-Plaza et al., 2001; Moreno de las Heras et al., 2010; Rosenbaum et al., 2012).

These factors make the water redistribution in the soil profile during the infiltration process and the flow generation mechanisms to change in time and space (Calvo-Cases et al., 2003), and they can lead to contrasting results when accomplishing water-oriented forest treatments. Integral assessments of both above- and belowground hydrological

processes following vegetation management are really scarce, especially in low-biomass semiarid forests. Such studies are needed in order to understand the relative importance of the driving factors and hence the efficiency and effectiveness of forest treatments in increasing soil drainage and deep-water storage under different climate and soil conditions.

Unmanaged high-density forests with low aboveground biomass (e.g. oak coppices and shrublands regenerated after wildfires) are common land-use covers in most dry regions such as eastern Spain, where they occupy about half of the forest area (DOGV, 2013). These areas are prone to climate-related disturbances (López et al., 2009, Doblas-Miranda et al., 2017), stressing the need to better define adaptive treatments for increasing watershed resilience. Likewise, in these water-scarce regions, aquifer recharge and other water-related issues have been identified as environmental services that should be targeted in forest planning and management (DOGV, 2013). Since forest treatments have already been proved to significantly increase net rainfall in these semiarid ecosystems (del Campo et al., 2018), it remains untested how this increase is actually allocated into soil water storage and other BHP. The experimental hypothesis is that the increased net precipitation through thinning/clearing of the low-biomass forests will enhance soil water replenishment, drainage and runoff at the plot scale. The major goal of this work is to study the effectiveness or the degree to which water-oriented forest treatments are successful in improving soil moisture and other BHP. This is assessed by comparing a thinning treatment with an un-thinned one in two forest types growing under contrasting environmental conditions but similar slope. To reach the major goal we address the following questions: i) What are the rainfall characteristics associated with different BHP as well as their relative contribution in explaining these processes together with that related to forest structure and antecedent soil water content?; ii) What is the net impact of

forest treatments on the magnitude and rate (as % of gross rainfall) of soil moisture, drainage and run-off?; iii) What are the short to mid-term trends and the cumulated effect in soil water, vertical and lateral flows following silvicultural interventions in the two contrasted forests? These results will help us to define properly forest management for improving water resources in these ecosystems.

2. Materials and methods

2.1. Study sites and treatments application

The study was carried out in two environmentally contrasted sites with marked differences in their climate-forest-soil aggrupation, although in both cases a low-biomass forest type (Pan et al., 2013) with high tree density and competition (overstocked) is present. Both sites are located in the Valencia province (E Spain) and distant about 100 km one to the other. The Calderona site (CAL, 39º42' N 0º27' W, 790 m a.s.l.), located within the Natural Park of "Sierra Calderona", has a marked influence of the Mediterranean Sea (25 km away), and the vegetation consists of an Aleppo pine (*Pinus halepensis* Mill.) stand of saplings with sparse shrubs, which was regenerated after a wildfire occurred in 1992. The south-westernmost site (HU, 39º04' N 1º14' W, 1090 m a.s.l.) is located in "La Hunde" public forest. This site has a more pronounced continental climate and it is occupied by a marginal oak coppice (*Quercus ilex* subsp. *ballota* (Desf.) Samp.). Both sites have been previously defined in terms of vegetation, climate, soils and other bio-geographical traits (del Campo et al., 2018, 2019). Table 1 summarizes key information according to the objectives of this work.

In each study site, detailed information about the depth and features of the soil-rock stratum (depth-to-rock, bedrock weathering and shallow groundwater routing) was gathered through a 2D electrical resistivity tomography (Samouëlian et al., 2005). The work consisted of twelve (six per site) 2D electrical tomographies with 48 electrodes,

following a Wenner-Schlumberger array configuration by using a Syscal Pro Switch resistivitymeter with 48 channels (Iris Instruments, Orleans, France). The 2D transects were processed at 2.5D to obtain a system of 3D geo-resistive volumes by the software of ERTLab Solver and RES2DINV (v.36.06).

In both sites no forest management has been carried out in the last decades. Juvenile thinning with shrub clearing were executed by a contractor of the Forest Service. The thinning removed the trees with smaller diameters and doubled-stemmed trees, trying to achieve a relatively homogeneous forest cover distribution. CAL was treated between January and October 2012, and HU in May 2012. Total basal area removed was 74% and 41% for CAL and HU, and the tree density reduction was of 94% and 73%, respectively (Figure 1, Table 2). Coarse woody debris were placed outside the plots, whereas fine woody debris were piled and grinded into mulch onto the plots. In each experimental site, a representative control plot with no thinning treatment and a contiguous thinned plot were established; each experimental plot having an area of 1500 m^2.

Forest structure was characterized in the experimental plots as detailed in del Campo et al. (2018). The variables considered were basal area (BA, m^2 ha^{-1}), tree density (De, trees ha^{-1}), forest cover (FC, %), leaf area index (LAI, m^2 m^{-2}) and diameters at basal and breast heights (D_B and D_{BH}, respectively, cm) (Table 2).

FIGURE 1

2.2. Rainfall and meteorological variables

Measurements were carried out from October 2013 to September 2016 in CAL and from October 2012 to September 2016 in HU. In each experimental site, a data-logging system was installed (CR1000, Campbell Sci., UT, USA) to register and store data, supplemented with two AM16/32B multiplexers, two SDM-IO16 expansion modules, a solar panel and

a 12 V battery. The system was programmed to read the sensors output every 5 s or 1 min and to record the values every 5 s or 10 min.

Gross rainfall (Pg) was continuously measured in each site at a height of 6 m above the ground by means of a tipping-bucket rain gauge with 0.2-mm resolution (7852, Davis Instruments Corp., Hayward, CA, USA). Rainfall events were classified according to a minimum time of 1 hour between two successive rains (Llasat, 2001) with at least 1 mm of rainfall depth (Muzylo et al., 2012). The following event variables were calculated for 10-minutes intervals: total rainfall depth (Pg, mm), duration (P_D, min), maximum and mean rainfall intensity (P_I and P_{Imx}, mm/h) and intra-event gaps as the proportion of time within the event with no rainfall (P_{Gap}, %). Also, in order to characterize the convective nature of the rainfall, we computed the β parameter (ratio of high intensity rainfall to total rainfall) for each rainfall event, adopting a threshold of 50 mm/h during 1 min (Llasat, 2001). For a time period of 10 min, this value dropped to 23.8 and 21.5 mm/h for CAL and HU, respectively. In this way, we computed the $\beta_{23.8,10}$ and $\beta_{21.5,10}$ parameters for each event and site (β=0 non-convective; 0<β≤S0.3 slightly convective; 0.3<β≤0.8 moderately convective and 0.8<β≤1.0 strongly convective).

The meteorological conditions during rainfall were characterized by measuring mean and maximum wind speed (U_{av} and U_{mx}, 7911 anemometer, Davis Instruments Corp.), air temperature and relative humidity (T, RH sensor, Decagon Devices, Pullman, USA) and vapour pressure deficit (VPD). Sensors were placed on the same mast as the rainfall gauge, and data were recorded in the same time intervals as those for rainfall.

Throughfall and stemflow were simultaneously measured as described in our previous work (del Campo et al. 2018). Stemflow was measured by sealing stem collars to 9-12 trees per treatment. After the plastic collars were attached, plastic tubes were inserted into small holes located in the lowest part of the collars to collect the water and divert it to

tipping-buckets (Pronamic 100.05) and then to 25-L deposits. Throughfall, was measured by setting out galvanized steel gutters per plot (9-15 per treatment), arranged following contour lines and maintained in the same positions throughout the study. The devices were set at 50 cm above the soil and sloping towards water counters (Altair V4, Diehl Metering) equipped with pulse counters. Net rainfall (Pn, mm) was computed for each event by the sum of throughfall plus stemflow, and rainfall interception was computed by subtracting net rainfall to Pg.

2.3. Soil water content and drainage

The electrical tomography revealed that soil depth was very low in most of the cases with the exception of the lower part in the plots of the CAL site, where a soil accumulation was present and therefore more water holding capacity is expected (Figure 2). This is in agreement with auger samplings and direct evidence from the observation of outcrops and stoniness in the plots. Therefore, the below-described layout of soil moisture sensors and piezometers was aimed to keep a comparable, balanced and equally depth-weighted deployment of readings between treatments and sites.

FIGURE 2

Soil water content (θ, $m^3 m^{-3}$) was continuously measured every 10 min, or every 5 s when raining, by means of FDR (frequency domain reflectometry or capacitive) probes (EC-5, Decagon Devices Inc., Pullman, WA) connected to a CR1000 data-logger. Sensors were installed by digging nine pits per plot (18 per experimental site) and grouped into three groups following contour lines. In each group, one of the pits contained two sensors poked horizontally at depths of 15 and 30 cm into the unaltered upslope pit face, whereas in the other two pits one sensor was inserted at 15 cm depth (12 sensors per plot, 24 sensors per experimental site). The pits were regularly placed following a mesh grid of 10 x 10 m in order to obtain a good estimate of mean soil water content (Molina et al., 2014). After

215 installation, the pits were backfilled with the excavated soils and slightly compacted up
216 to similar bulk density to that of unaltered soil. Calibrations were discarded as the
217 observed increase in θ after calibrating some sensors was offset when taking into account
218 the stoniness effect in field conditions, and because of the temporal drifts observed in
219 several cases, preventing the use of a static calibration curve; thus, we used default
220 calibration (for mineral soils) in all cases (Detty and McGuire, 2010).
221 For each rainfall event and probe, we considered the first (θ_{st}) and the maximum (θ_{mx})
222 values of soil moisture. Field capacity for each probe (θ_{fc}) was calculated for gentle
223 rainfall events (>20 mm, usually the daily rainfall was much higher because of the
224 threshold considered for separating events), collected at night-time, by averaging the
225 (steady) values of θ during at least four hours once the exceeding water was lost. The
226 steady values were assessed to be preceded by a steep decrease (exceeding water) and
227 then reaching a constant value during at least four hours without rainfall at night time (the
228 decrease rate in 240 min was found to be less than 0.0034 and 0.0027 m3/m3 for
229 Calderona and La Hunde sites respectively). However, we observed that these θ_{fc} values
230 were not persistent as some probes showed temporal drifts (means ± standard deviations
231 during the study period were 0.167±0.043 m3/m3 and 0.192±0.037 m3/m3 for CAL and
232 HU, respectively). Thereafter, we recomputed θ_{fc} for each sensor whenever Pg surpassed
233 the established 20 mm threshold (9 and 13 times for CAL and HU, respectively).
234 Soil water replenishment ($\Delta\theta$, $m^3\ m^{-3}$) around a probe was computed for every rainfall
235 event as the difference between the θ maximum and first values, as $\Delta\theta = \theta_{mx} - \theta_{st}$ when
236 field capacity was not reached or as $\Delta\theta = \theta_{fc} - \theta_{st}$ when it was. $\Delta\theta$ data were converted to
237 $\Delta\theta$ depth (mm) by considering the soil column depth. When looking at the wetting process
238 of the soil profile, we observed in our dataset that soil depth differences were irrelevant,
239 showing a non-uniform behaviour probably led by preferential vertical channels through

240 macropores (Calvo-Cases et al., 2003; Lin and Zhou, 2008). Thus, we decided to use the
241 weighted depth of the moisture sensors (187.5 mm) to calculate soil water replenishment
242 for each sensor and subsequently average across the 12 probes to obtain the $\Delta\theta$ depth for
243 each experimental plot. Values of $\Delta\theta$ calculated in this way are likely to be
244 underestimated, as hydrological processes at the upper soil layers are not fully addressed
245 (e.g. light-rainfall events, litter interception, higher soil moisture holding capacity in the
246 upper organic horizons, etc.).
247 Drainage (D, mm) was estimated based on θ and Pg observations. For each probe, all Pg
248 collected when the probe was above θ_{fc} was considered drainage. Rainfall interception
249 was assumed to have already taken place by the time the sensors reached θ_{fc}. In case the
250 resulting drainage amount was higher than the mean net precipitation estimated for the
251 experimental plot (del Campo et al., 2018), then D was reset to that value. In case there
252 was run-off (see below), it was deducted from D. We established a threshold to consider
253 a spatially generalized drainage (Dgen, mm) by considering a minimum of 2/3 out of the
254 12 FDR sensors showing values above θ_{fc} in each experimental plot. As different sensors
255 entered into field capacity at different moments, we considered the mean Pg from these
256 *active* sensors for calculations. Drainage calculated in this way is independent from the
257 above-mentioned uncertainty in calculating $\Delta\theta$ depth and only depends on field capacity
258 and Pg, both with a more robust estimation. Also, the difference D-Dgen can be
259 considered as a surrogate of soil water storage below 18.75 cm.
260 In addition, four 10 cm-diameter piezometers (from 1 to 4 m depth) were drilled at the
261 downslope side of each experimental plot (eight per site) according to the information
262 from tomography. These wells were aimed to detect deep infiltration and validate the
263 estimations of drainage based on θ and Pg observations. A slotted screen PVC pipe was
264 inserted into each well that was blind on its top 60 cm to avoid shallow flows getting in.

Also, a 10 cm layer of coarse bentonite was inserted at the top of the well around the pipe. Every 1-3 weeks (depending on rainfall), we made qualitative checks of groundwater movement by visual identification of the water depth in a transparent bailer placed inside the wells (Model 428 BioBailer, ESP ltd.). Malfunctioning of the bailer in HU during most of time led to implement automatic readings of water level (PX40-15G5V, Omega Eng. ltd.) in both sites at the end of the study period, thus allowing for a more reliable validation of the estimations.

2.4. Lateral soil water flow

Lateral soil water flow was collected by 30-40 cm depth trenches dug downslope in each experimental plot. The upslope side of the trenches was open to subsurface flows by attaching a fine mesh filter directly to the ground exposed to air (downslope and base sides of the trench were water-proofed with concrete) (Figure 1). The surface and subsurface flows (hereinafter considered as runoff, RO, to give more fluency to text) collected were diverted to deposits equipped with automatic pulse counters (Altair V4, Diehl Metering, minimum flow rate 5 l h^{-1}). Two 6 m long ditches per experimental plot were dug in HU, whereas in CAL a single 35 m long ditch per experimental plot was dug edging the lower boundary of the plots. The measurement time lapse was set to 5 s (raining) or 10 min (no raining). Similar trenches were dug upslope on the upper boundary of the plots in order to divert off the run-on onto the plots.

2.5. Data treatment and analysis

Data were quality-controlled for spikes and gaps (del Campo et al., 2018). To study the relative contribution of rainfall, meteorological conditions during rainfall, antecedent soil moisture and forest structure to the different BHP ($\Delta\theta$, D, Dgen, and RO), boosted regression trees models (BRT) were performed in R software (RStudio Team, 2015), using the ‘‘gbm” package (Ridgeway, 2017; Elith and Leathwick, 2017). In the BRT

290 analysis, a Gaussian distribution family, learning rate of 0.005, tree complexity of 4-5,
291 and bag fractions of 0.6-0.75 were considered. The minimum number of trees was in all
292 cases above 1500. The results of this analysis provided the relative influence (RI) of the
293 predictors on the response variable. This measures the number of times a predictor
294 variable is selected for splitting, weighted by the squared improvement in the model as a
295 result of each split, averaged over all trees, and scaled so that the sum adds to 100 (Elith
296 et al., 2008). The higher the RI, the stronger the influence of the predictor in the response
297 variable.
298 The effect of the forest treatment on depth and rates of the response variables ($\Delta\theta$, D,
299 Dgen, and RO), was analysed in each site through an ANCOVA analysis considering
300 treatment as factor and Pg as covariate. θ_{st} and θ_{mx} were also included in this analysis
301 after normalizing them to their relative values (θ_{st_rel} and θ_{mx_rel}, %, dividing their current
302 values by the overall range of each probe during the monitoring period). Because of the
303 inevitable heterogeneity of soil properties among different probes (texture, stoniness and
304 bulk density) makes that the water holding capacity of the soil may change, this
305 normalization ensures that the comparison between thinning and control treatments is
306 unbiased. Data were examined for normality, homoscedasticity and homogeneity in the
307 regression slopes and transformed with power functions if necessary or, alternatively, a
308 non-parametric Kruskal–Wallis test based on the chi-squared statistic was used.
309 Cumulative treatment impacts on the response variables were evaluated in terms of a shift
310 of the daily ratio of thinned/control following the intervention: L (T/C) (Perry and Jones,
311 2017). The water balance of net rainfall (Pn, mm) for each water year and experimental
312 plot was calculated as: $Pn = RO + \Delta\theta + D + U$, where Pn is the annual cumulated value
313 of the sums of throughfall and stemflow for each rainfall event calculated in del Campo
314 et al. (2018); RO is the annual cumulated runoff value; D is the annual cumulated value

315 of drainage; $\Delta\theta$ is the annual cumulated value of soil water replenishment; and U is an
316 unexplained term which cannot be explained and is mostly influenced by hydrological
317 processes taking place in the uppermost soil layers (soil water replenishment in the upper
318 organic layers and interception from litter, grass and dwarf shrubs).
319 Finally, in a context of rainfall scarcity and irregularity, the effectiveness of the treatment
320 can be assessed through observing the proportionality of the change in a target
321 hydrological process with regards to the change in Pg. To that end we performed an
322 elasticity analysis for soil moisture and drainage in order to address how the annual
323 variability in Pg is translated into relative changes in these key hydrological variables,
324 and how the treatment affected it. The mean annual θ_{mx_rel}, the cumulated annual Dgen
325 and the ratio (Dgen+RO)/(Pg-Dgen-RO) as a proxy to the blue/green water ratio
326 (González-Sanchis et al., 2015) were used in this analysis. To that end, we used a similar
327 approach to that of Jiang et al. (2014) but comparing the different water years with the
328 wettest one instead of using the average of the series. We mostly registered dry years in
329 both sites, so by doing this selection we remain close to the expected average (Table 1),
330 and at the same time we tested for changes towards drier conditions. Elasticity (e) is
331 defined then as the proportional change in a given hydrologic variable (X) in response to
332 the proportional change in annual precipitation, and it is expressed as:
333 e_X = Median [(Xt-Xw) / (Pt-Pw) * Pw/Xw]
334 where Xw and Pw are the totals of the hydrologic variable and the precipitation in the
335 wettest water year of the series, and Xt and Pt are totals of the variable and precipitation
336 at any other given year t, respectively. High degree of elasticity (e>1) means that the
337 variable X is very sensitive or vulnerable to a proportional change in P; unit elasticity
338 (e≈1) means that a relative change in P is translated into a proportional change in a given
339 variable (X); low elasticity (e<1) or inelastic (e≈0), occurs when little or no change is

detected in the hydrological variable for a given change in P. This simple approach helps to uncover, directly from observational data, the direction and strength with which different hydrological variables respond to declining P either under managed or unmanaged scenarios (Jiang et al., 2014).

3. Results

3.1. Characteristics of gross rainfall and meteorological conditions

Gross rainfall results have been also reported in del Campo et al. (2018). Briefly, total Pg in CAL was 162, 370 and 246 mm for the water years 2013-2014 to 2015-2016 respectively, whereas 534, 271, 426 and 297 mm for the years 2012-2013 to 2015-2016, respectively in HU. Non-convective rainfall events presented higher depth and duration in HU (Table 3); however, Pg presented a higher convective pattern in CAL, with 38% of total Pg fallen in this class (11% in HU), and higher Pg, P_D, P_I and P_{Imx}. Furthermore, the convective rainfall events were accompanied with more evaporative conditions (Table 3).

The number of events that provoked either drainage or runoff regardless of the treatment was higher in HU (118-149) when comparing with the coastal site of CAL (25-41) (Table 3). In HU, it is remarkable that the features of these events were only slightly higher than the average rainfall event (Table 3): the ratio to the average event ranged between 1.2 and 1.5 for depth, duration and intensity. In contrast, there was a clear departure of these events from the depth, duration and intensity of the average event in CAL (multiplicative factor between 1.5 to more than 3.0). These differences in the threshold of Pg that trigger the different hydrological processes between both sites were also associated to different antecedent soil water conditions (see below).

3.2. Influence of rainfall, meteorology, forest structure and antecedent soil moisture on soil water replenishment, drainage and runoff

The four sets of independent variables considered (rainfall characteristics: Pg, P_D, P_I, P_{Imx}, P_{Gap}, β; meteorology during the event: T, VPD, RH, U_{mx}, U_{av}; forest structure: FC, BA, LAI, De; and antecedent soil moisture θ_{st_rel}), presented significant correlations with the studied BHP ($\Delta\theta$, D, Dgen and RO) in both sites (Table 1S in supplementary material). The analyses performed through BRT models yielded better cross-validation correlations for the depth-expressed (mm) variables than when they were expressed by rates (% Pg), and those tested for CAL showed better fits than for HU in both cases (Table 4). The relative importance (RI) of the four sets of independent variables on explaining the hydrological processes is shown in Figure 3, weighted by the corresponding correlation coefficients from Table 4 (Figure 3S shows the RI individually for the most influential independent variables). It is remarkable in Figure 3 the overwhelming importance of the rainfall variables (mostly Pg, followed by P_D and P_{Imx}) on the magnitude (mm) of the different BHP, with a cumulative RI between 30-76%, depending on the site/dependent variable. On the contrary, the contribution of these variables to the rates was modest regardless of the site (cumulative RI between 5-29%). The meteorological conditions during rainfall and the antecedent soil moisture showed modest RI's for depths (2-21% and 5-25% in CAL and HU respectively) but increased their RI for rates in both sites (between 11-43%). Forest structure remained with low RI whatever the case, although it improved when combining both sites in the model (RI for $\Delta\theta$ as % Pg was 8.3%)

FIGURE 3

3.3. The effects of thinning on soil water, drainage and runoff

3.3.1. Effects at the event scale

The difference between thinned and control plots for the different variables describing the net rainfall redistribution processes was tested through ANCOVA test (see Table 2S for a summary of the analyses). CAL presented only significant differences in relative

soil water content both at the first (θ_{st_rel}) and the maximum (θ_{mx_rel}) values, showing higher values in the thinned plot (Figure 4); thus, no further effect of thinning was significantly detected in CAL, although the averages of $\Delta\theta$, D, Dgen and RO were higher in the thinned plot (Figure 5). In contrast, the thinned plot in HU presented significant differences with the control in all the BHP considered except for RO (Table 2S, Figures 4 and 5).

FIGURE 4

FIGURE 5

3.3.2. Temporal dynamics and annual balances

The temporal dynamics of $\Delta\theta$, D, Dgen and RO for both plots and sites are shown in Figures 6 to 8. Regarding RO, although it represented less than 1% of total Pg, its dynamics were markedly different between the sites. CAL presented very few RO events, basically responding to high-intensity storms (Table 3) and showing in some cases overland hortonian flow (e.g. the event in Aug 10th, 2016 with Pg=19.0 mm, β=0.41, P_D=167 min, P_{Imx}=32.1 mm/h, P_I=6.8 mm/h). In contrast, RO in HU was observed within a higher range of rainfall characteristics, indicating a higher dependency on antecedent soil moisture content (e.g., an event observed in Jan 29th, 2014 with only 2.8 mm of Pg generated RO in both the control and thinned plots).

Regarding the dynamics on drainage flows, Figure 8 shows that CAL presented a more static pattern with little or no differences in either D or Dgen between both plots ($\ln(Dgen_T/Dgen_C)\approx0$), but a clear differentiation in HU for this flow, in agreement with the results of the ANCOVA. With regards to $\Delta\theta$, the lower θ_{st} in the control plot in HU made more infiltrated water to be allocated into soil water replenishment (so that $\ln(\Delta\theta_T/\Delta\theta_C)<0$, Figure 8), whilst higher θ_{st} in the thinning treatment (closer to θ_{fc}) reduced the availability for soil water storage. In contrast, θ_{st} in CAL was lower in both plots and

416 the increased Pn led by thinning was almost fully allocated to increase this state variable,
417 thus making the series $\ln(\Delta\theta_T/\Delta\theta_C)>0$ (Figure 8). Also, whereas in HU the temporal
418 pattern showed a diminishing trend of the series $\ln(\Delta\theta_T/\Delta\theta_C)$ with time, CAL presented a
419 static pattern mainly due to the lack of rainfall (Figures 6 and 8).
420 The comparisons between the underground water movement from observations in the 1-
421 4 m depth piezometers and the estimations of drainage flows based on θ and Pg agreed
422 well in both sites and plots (Figures 6 and 7), thus validating the occurrence of D and
423 Dgen. In CAL, the rise of the water level in the piezometers during the period they were
424 monitored matched 100% of the events presenting either D or Dgen in the thinned plot,
425 and most of the estimated D (95%) and Dgen (95%) was paired with a response in the
426 wells for the control plot. In HU, with less validation period, the wells responded for 92%
427 of the calculated D flow in either plot, and 96% of Dgen in the thinned plot; however, the
428 lower matching between the response of the piezometers and Dgen in the control plot,
429 means that in this site with shallow soil, higher Ks and organic matter (Table 1), D is a
430 good estimator of total drainage.

431 FIGURE 6

432 FIGURE 7

433 FIGURE 8

434 The annual balances in Figure 9 represent the cumulative values of the BHP (RO was
435 negligible in all cases and therefore not represented) sorted by water years, sites and plots.
436 It is remarkable how the cumulative Pn increase led by thinning was differently translated
437 into Δθ and drainage, thus agreeing the previous event-based results. In CAL, D was very
438 similar between the experimental plots (mean values of 89 *vs.* 97 $mm \cdot year^{-1}$ for C and T
439 respectively), whereas in HU percolation was always higher in the thinned plot (mean
440 values were 118 *vs.* 169 $mm \cdot year^{-1}$ for C and T, respectively). In contrast, the differences

441 in $\Delta\theta$ between T and C ranged from 10 to 52 mm in CAL and between -9 and -75 mm in
442 HU. In addition, the unexplained term ranged between 23-51 mm (8-31% of Pn) in CAL
443 and 2-114 mm (2-29% of Pn) in HU.

444 FIGURE 9

445 *3.3.3. Elasticity analysis*

446 The elasticity analysis indicated that the implementation of silvicultural treatments
447 improved the elasticity for Dgen and the ratio blue/green water (B/G) in dry years with
448 regards the reference year (near the average Pg) (Figure 10). By sites, in HU higher
449 vulnerability in Dgen and B/G in the control ($e>1.65$) in dry years turned into a more
450 proportionate change to Pg when management took place ($e\approx1$). In CAL, with very low
451 values observed in both plots either for Dgen or B/G, the thinning treatment changed the
452 elasticity from vulnerable ($e=1.25$ in Dgen) or insensitive ($e=0.68$ in B/G) to elastic for
453 both variables ($e\approx1.1$). Regarding θ_{mx_rel} (i.e., the maximum soil hydration achieved in an
454 event, relativized, so that soil properties do not affect this value), forest management
455 turned it more insensitive ($e<1$) to Pg decreasing. In this sense, as the thinning improved
456 significantly θ_{mx_rel} in both sites, this change in elasticity is certainly desirable (soil
457 moisture is still higher despite years become drier).

458 FIGURE 10

459 **4. Discussion**

460 A previous work regarding the effects of thinning on rainfall partitioning (del Campo et
461 al., 2018) showed that the reduction of forest biomass led to significant effects on net
462 rainfall (Pn) in both study sites, increasing from 554 to 634 mm in CAL and from 1088
463 to 1294 mm in HU when looking at the cumulated values in C and T respectively within
464 the same study period (cumulated Pg was 779 and 1528 mm for CAL and HU,
465 respectively). The present work is thus focused on further studying the distribution of Pn

into soil, finding that thinning affected most of the belowground hydrological processes (BHP) in a contrasted way between both sites, which confirms partially our hypotheses.

4.1. Driving variables of the belowground hydrological processes

Forest cover reduction through thinning enhances Pn mainly due to an increase in throughfall (Chirino et al., 2006; Molina and del Campo, 2012; del Campo et al., 2018), so that the question that arises is how this increased throughfall is partitioned into the different BHP (Coenders-Gerrits et al., 2012). In our case, the different types of independent variables considered in the BRT were shown to affect these BHP to contrasted extents when expressing the variables either as depth or rate. However, forest structure showed very low RI in either case, which contrasts with the significant effects observed in the ANCOVA's. In order to explain this conflicting result, we must pay attention to the antecedent soil moisture (θ_{st_rel}), which was significantly improved by 10% (about 5% in absolute value) with the thinning treatment (Figure 4), and it was the most important variable in explaining the rate of Pg which is diverted into the different BHP (RI of 29% on average, Figure 3). This means that the eco-hydrological impact of forest management should be better evaluated in terms of changes in the soil water content, which is in fact one of the most important changes following thinning treatments (Breda et al., 1995; del Campo et al., 2014; Cabon et al., 2018; del Campo et al., 2019).

Other independent variables were also brought up in the BRT as key drivers of the different BHP. The control that rainfall exercises on the magnitude of water components in soils is recognized elsewhere (Calvo-Cases et al., 2003; Chirino et al., 2006; Owor et al., 2009; Bachmair et al., 2012), and in our case, it played the most important role in explaining the depth-expressed variables (RI>75% in some cases, Figure 3), with the magnitude of Pg being by far the most explicative variable, followed by P_D, P_{Imx} and β (Figure 3S). From these results, it can be deducted that certain thresholds and patterns in

491 the rain features and meteorology that characterize a particular rainfall regime are
492 important on evaluating the effectiveness of water-oriented forest treatments. For
493 instance, the partial dependence of $\Delta\theta$ on rain convection presents a threshold at about
494 $\beta>0.3$ (Figure 3S).

495 *4.2. Lateral soil water flow*

496 Runoff in mature forest stands or wooded vegetation ecosystems with high biomass
497 quantity is generally low given both the high soil organic carbon content and the high
498 infiltration capacity led by macropores (Beven and Germann, 2013). Chirino et al. (2006)
499 obtained runoff coefficients less than 1% of Pg in a 30-year-old semiarid Aleppo pine
500 plantation, while Merino-Martin et al. (2012) and Moreno-de las Heras et al. (2010)
501 observed runoff coefficients less than 4.5 % in a reclaimed slope with natural regenerated
502 grassland covering more than 50% of soil. In our case, the mean annual coefficients
503 remained below 1% of gross rainfall for C and T plots in both sites, and they accounted
504 not only for runoff, but also for subsurface flows. Cerdá et al. (2017) reported values of
505 this water component averaging 8.3% of Pg on Aleppo pine and 1.4% on Holm oak plots
506 ($1m^2$) in a site similar to that of CAL regarding soil, vegetation and meteorological
507 conditions (slope gradient was not reported). The required depth of an event in CAL (pine
508 stand) to originate runoff (mean of 16.3 mm, Table 3) was lower than in the referred work
509 (minimum of 18.7 mm) despite the fact that runoff was much higher in that study. In this
510 respect, scale effects (1500 *vs.* 1 m^2) seem to be the most likely reason of this discrepancy.
511 Moreno-de las Heras et al. (2010) reported in a dry Mediterranean site with similar soil
512 organic matter to ours, a generalized decrease of 79% in runoff per unit area with
513 increasing slope length from 1 to 15 meters. As these authors pointed out, the locally
514 generated runoff re-infiltrates farther downslope depending on soil degradation, micro-
515 topography and rainfall conditions, and the same factors together with the macroporosity

structure are expected to control subsurface flows (Lin and Zhou, 2008). Our data on soil water content suggest an important macropore flow, with similar values between the FDR probes at different depths regardless the time during several rainfall events. By the same, the available automatic readings from the piezometers showed that deep infiltration began almost simultaneously with rainfall (Figure 4S).

In this regard, the results indicate that thinning did not significantly affect the soil characteristics in the uppermost layers controlling surface and subsurface water flows, given our non-significant differences on RO (Figure 5 and Table 2S). In this sense, measurements of ponding and tension infiltration in the holm oak site (HU) confirmed that both saturated and unsaturated hydraulic conductivity were not significantly different between the plots (di Prima et al., 2017).

4.3. Soil moisture replenishment and drainage

The most relevant finding observed in the present study is the differential effect that thinning produced in $\Delta\theta$ and drainage between both sites (Figures 6 to 8). Increased Pn in the thinned plot of CAL led to higher $\Delta\theta$ in a relatively dry soil (θ_{st_rel}=45%), but negligible or little further movement of this water below the upper soil layers. The reason is that less and sparser rainfall events together with higher evaporative conditions in this site provoked low antecedent soil water content in both plots, and hence significant amounts of net precipitation were required to surpass θ_{fc} (full soil water replenishment). Consequently, only those rainfall events with enough volume were able to gently overcome that threshold (mean Pg for Dgen was 13 mm), but at the same time these showers quickly saturate the canopy resulting in little differences in Pn between C and T, so that θ_{fc} is exceeded in either case, and drainage was non-significantly different between plots. In contrast, HU showed a marked rainy season with low evaporative conditions, leading to higher θ_{st} (θ_{st_rel}=66%) in the thinning treatment, and the increased Pn here

moved downward as drainage, as θ_{fc} was surpassed in more rainfall events (mean Pg for Dgen was 7 mm). Drainage is usually associated to consecutive rainy days out of the growing season (García-Prats et al., 2016), a pattern that is almost absent in the drier site of CAL. The important consequence is that, when managing forests for increasing infiltration (Ungar et al., 2013; del Campo et al., 2014; Ilstedt et al., 2016), changes in the soil moisture regime are the critical factor that triggers when the increased Pn after thinning turns into deep water reservoir. It must be stated that the drainage rates measured in our plots do not necessarily reflect current recharge rates to downslope streams or water tables, but rather deep-water storage for ET, as plant-water uptake cannot be considered negligible at the depths observed in our plots (del Campo et al., 2019).

4.4 Temporal dynamics and elasticity

In the drier site of CAL, both low rainfall and the subsequent slow growth of the vegetation have made the temporal series L (T/C) remaining with little change for the BHP, as already observed for the rainfall partitioning (del Campo et al., 2018). On the other hand, in HU L (T/C) showed changing temporal trends in the BHP reflecting the impact of wet/dry spells, together with the combined effect of tree growth especially in the thinned plot (del Campo et al., 2019): L (D_T/D_C) remained relatively steady along the 4-year period, whereas in the case of Dgen, it can be observed in Figure 8 that T and C did not differ in the driest spell of 2013-2014 (L ($Dgen_T/Dgen_C$)≈0), although when wetter conditions returned, the series became positive again. This absence of differences under dry conditions shows similar pattern to that observed in CAL and has also been previously modelled for Aleppo pine in HU (González-Sanchis et al., 2015). It is also worth to mention that during this dry spell (Aug-2013 to Oct-2014), the series L ($\Delta\theta_T/\Delta\theta_C$) becomes more negative, indicating that the drier soil in the control retains more net rainfall as $\Delta\theta$, whereas the opposite pattern for L (D_T/D_C) indicates more water allocated

to drainage in the thinning treatment. This implies that even in dry years, deep soil moisture is improved with thinning, a fact that was brought up in the elasticity analysis. From late 2014 on, the growth of the oaks speeded up in the cleared plot and further affected soil moisture patterns (del Campo et al., 2019).

Vegetation management in semiarid shrublands is known to be of limited effectiveness when aiming to increase water yield at the catchment scale (Bosch and Hewlett, 1982; Hibbert et al., 1982), but it may be certainly opportune when dealing with global change-induced impacts by enhancing ecosystem resilience (Grant et al., 2013; Lindner et al., 2014; Seidl et al 2016). In this sense, our results proved that the irregular and dry conditions that prevailed throughout the study impacted differently in control and thinned plots as revealed on the elasticity of key eco-hydrological variables (soil moisture and deep-water reservoir). Although the comparison between control and thinning treatments is objective and robust, some uncertainty still persists in our study, as part of the net rainfall was unexplained when totalizing the studied BHP. Since our sensors were installed at 15 and 30 cm depth, soil evaporation from the surficial layers and litter interception are likely the most contributing factors to this unexplained term, given their importance in semiarid environments (Tsiko et al., 2012; del Campo et al., 2019). Therefore, further measurements are required to fully account for soil water content variation.

5. Conclusions

Proactive-adaptive silviculture needs to be necessarily eco-hydrologically oriented in the case of semiarid regions. Our work evaluated the short-term effect of thinning on the redistribution of net rainfall into the soil of two semiarid forests with contrasted rainfall and vegetation characteristics. Lateral water flows were negligible and not significantly affected by tree removal in either site, so the protective role of forest in controlling soil

591 erosion was not modified through thinning. In contrast, soil water replenishment and
592 drainage were affected to different extents depending on the site, highlighting that, under
593 the same semiarid climate and low-biomass vegetation, responses to water-oriented
594 treatments can be very different according to local/regional variations in climate and
595 forest-types: while in the most arid conditions thinning improved soil water content and
596 made it more independent from annual changes in Pg, drainage was only enhanced in the
597 wetter site (HU) given the higher antecedent soil water conditions. Thus, under the
598 expected global change-induced impacts on vegetation due to increased soil water
599 shortage in semiarid environments, biomass reduction seems to be an effective tool for
600 adapting forest, and in some cases, also for increasing deep soil water reservoirs. Further
601 questions to be addressed are the mid-term duration of the effects and the intensity of the
602 treatments, the later to test whether drainage can be positively affected in the most arid
603 conditions when higher biomass reduction is considered.
604

605 **Acknowledgements**

606 This study is a component of research projects: HYDROSIL (CGL2011-28776-C02-02),
607 SILWAMED (CGL2014-58127-C3-2), CEHYRFO-MED (CGL2017-86839-C3-2-R)
608 funded by the Spanish Ministry of Science and Innovation and FEDER funds and LIFE17
609 CCA/ES/000063 RESILIENTFORESTS. The authors are grateful to the Valencia
610 Regional Government (CMAAUV), VAERSA, ACCIONA, the "Sierra Calderona"
611 Natural Park and the communal authority of Serra, for their support in allowing the use
612 of the experimental forest and for their assistance in carrying out the fieldwork. A.J.
613 Molina is beneficiary of a "Juan de la Cierva" post-doctoral fellowship funded by the
614 Spanish Ministry of Economy and Competitiveness.

615 **References**

Allen, C.D., Macalady, A.K., Chenchouni, H., Bachelet, D., McDowell, N., Vennetier, M., Kitzberger, T., Rigling, A., Breshears, D.D., Hogg, E.H., Gonzalez, P., Fensham, R., Zhang, Z., Lim, J.H., Castro, J., Demidova, N., Allard, G., Running, S.W., Semerci, A., Cobb, N., 2010. A global overview of drought and heat-induced tree mortality reveals emerging climate change risks for forests. For. Ecol. Manage. 259, 660– 684.

Bachmair, S., Weiler, M., Troch, P. A., 2012. Intercomparing hillslope hydrological dynamics: Spatio-temporal variability and vegetation cover effects. Water Resour. Res. 48, W05537. doi:10.1029/2011WR011196.

Beven, K., Germann, P., 2013. Macropores and water flow in soils revisited. Water Resour. Res. 49, 3071-3092.

Bosch, J.M., Hewlett, J.D., 1982. A review of catchment experiments to determine the effects of vegetation changes on water yield and evapotranspiration. J. Hydrol. 55, 3-23.

Bréda, N., Granier, A., Aussenac, G., 1995. Effects of thinning on soil and tree water relations, transpiration and growth in an oak forest (Quercus petraea (Matt.) Liebl.). Tree Physiol. 15, 295–306.

Cabon, A., Mouillot, F., Lempereur, M., Ourcival, J.M., Simioni, G., Limousin, J.M., 2018. Thinning increases tree growth by delaying drought-induced growth cessation in a Mediterranean evergreen oak coppice. For. Ecol. Manage. 409, 333-342.

Calvo-Cases, A., Boix-Fayos, C., Imeson, A. C., 2003. Runoff generation, sediment movement and soil water behaviour on calcareous (limestone) slopes of some Mediterranean environments in southeast Spain. Geomorphology 50, 269-291.

Cerdà, A., Lucas-Borja, M.E., Úbeda, X., Martínez-Murillo, J.F., Keesstra, S., 2017.

638 *Pinus halepensis* M. versus *Quercus ilex* subsp. *rotundifolia* L. runoff and soil erosion at
639 pedon scale under natural rainfall in Eastern Spain three decades after a forest fire. For.
640 Ecol. Manage. 400, 447–456

641 Chirino, E., Bonet, A., Bellot, J., Sánchez, J. R., 2006. Effects of 30-year-old Aleppo
642 pine plantations on runoff, soil erosion, and plant diversity in a semi-arid landscape in
643 south eastern Spain. Catena. 65, 19-29.

644 Coenders-Gerrits, A.M.J., Hopp, L., Savenije, H.H.G., Pfister, L., 2012. The effect of
645 spatial throughfall patterns on soil moisture patterns at the hillslope scale. Hydrol. Earth
646 Syst. Sci. Discuss. 9, 8625–8663.

647 Creedy, J., Wurzbacher, A.D., 2001. The economic value of a forested catchment with
648 timber, water and carbon sequestration benefits. Ecol. Econ. 38(1), 71-83.

649 Crockford, R.H., Richardson, D.P., 2000. Partitioning of rainfall into throughfall,
650 stemflow and interception: effect of forest type, ground cover and climate. Hydrol.
651 Process.14, 2903-2920.

652 del Campo, A.D., Fernandes, T.J.G., Molina, A.J., 2014. Hydrology-oriented (adaptive)
653 silviculture in a semiarid pine plantation: How much can be modified the water cycle
654 through forest management? Eur. J. For. Res. 133(5), 879-894.

655 del Campo, A.D., González-Sanchis, M., Lidón, A., Ceacero, C., García-Prats, A., 2018.
656 Rainfall partitioning after thinning in two low-biomass semiarid forests: impact of
657 meteorological variables and forest structure on the effectiveness of water-oriented
658 treatments. J. Hydrol., 565: 74-86.

659 del Campo, A.D., González-Sanchis, M., Garcia-Prats, A., Ceacero, C.J., Lull, C. 2019.

660 The impact of adaptive forest management on water fluxes and growth dynamics in a
661 water-limited low-biomass oak coppice. Agric. For. Meteorol. 264: 266–282.

662 Detty, J.M., McGuire, K.J., 2010. Topographic controls on shallow groundwater
663 dynamics: implications of hydrologic connectivity between hillslopes and riparian zones
664 in a till mantled catchment. Hydrol. Process. 24, 2222–2236.

665 Devitt, D.D., Smith, S.D., 2002. Root channel macropores enhance downward
666 movement of water in a Mojave Desert ecosystem. J. Arid Environ. 50, 99-108.

667 di Prima, S., Bagarello, V., Angulo-Jaramillo, R., Bautista, I., Cerdà, A., del Campo, A.,
668 González-Sanchis, M., Iovino, M., Lassabatere, L., Maetzke, F., 2017. Impacts of
669 thinning of a Mediterranean oak forest on soil properties influencing water infiltration.
670 J. Hydrol. Hydromech. 65, 276–286.

671 Doblas-Miranda, E., Alonso, R., Arnan, X., Bermejo, V., Brotons, L., de las Heras, J.,
672 Estiarte, M., Hódar, J. A., Llorens, P., Lloret, F., López-Serrano, F. R., Martínez-Vilalta,
673 J., Moya, D., Peñuelas, J., Pino, J., Rodrigo, A., Roura-Pascual, N., Valladares, F., Vilà,
674 M., Zamora, R., Retana, J., 2017. A review of the combination among global change
675 factors in forests, shrublands and pastures of the Mediterranean Region: Beyond
676 drought effects. Glob. Planet. Change 148, 42-54.

677 DOGV, 2013. DECRETO 58/2013, de 3 de mayo, del Consell, por el que se aprueba el
678 Plan de Acción Territorial Forestal de la Comunitat Valenciana. [2013/4617].
679 DOGV núm. 7019 de 08.05.2013.

680 Dung, B. X., Gomi, T., Miyata, S., Sidle, R. C., Kosugi, K., Onda, Y., 2012. Runoff
681 responses to forest thinning at plot and catchment scales in a headwater catchment
682 draining Japanese cypress forest. J. Hydrol. 444, 51-62.

683 Elith, J., Leathwick, J.R., Hastie, T., 2008. A working guide to boosted regression
684 trees. J. Anim. Ecol. 77(4), 802–813.

685 Elith J., Leathwick J., 2017. Boosted regression trees for ecological modelling.
686 https://cran.r-project.org/web/packages/dismo/vignettes/brt.pdf (last accessed 10.05.18)

687 Ellison, D., Morris, C.E., Locatelli, B., Shell, D., Cohen, J., Murdiyarso, D., et al. 2017.
688 Trees, forests and water: Cool insights for a hot world. Global Environ. Change 43, 51-
689 61.

690 Fernandes, T. J., del Campo, A. D., Herrera, R., Molina, A. J., 2016. Simultaneous
691 assessment, through sap flow and stable isotopes, of water use efficiency (WUE) in
692 thinned pines shows improvement in growth, tree-climate sensitivity and WUE, but not
693 in WUEi. For. Ecol. Manage. 361, 298-308.

694 Ganatsios, H.P., Tsiorasb, P.A., Pavlidisa, T., 2010. Water yield changes as a result of
695 silvicultural treatments in an oak ecosystem. For. Ecol. Manage. 260 (8), 1367-1374.

696 García de la Serrana, R., Vilagrosa, A., Alloza, J. A., 2015. Pine mortality in southeast
697 Spain after an extreme dry and warm year: interactions among drought stress,
698 carbohydrates and bark beetle attack. Trees 29, 1791-1804.

699 García-Prats, A., del Campo, A., Fernandes, T.J.G., Molina, A., 2015. Development of a
700 Keetch and Byram-based drought index sensitive to forest management in
701 Mediterranean conditions. Agric. For. Meteorol. 205, 40-50.

702 García-Prats, A., del Campo, A. D., Pulido-Velazquez, M., 2016. A hydroeconomic
703 modeling framework for optimal integrated management of forest and water. Water
704 Resour. Res. 52, 8277–8294.

705 Gómez-Plaza, A., Martínez-Mena, M., Albaladejo, J., Castillo, V.M. 2001. Factors
706 regulating spatial distribution of soil water content in small semiarid catchments. J.
707 Hydrol. 253, 211-226.

708 González-Sanchis, M., del Campo, A., Molina, A.J., Fernandes, T.J.G., 2015. Modeling
709 adaptive forest management of a semi-arid Mediterranean Aleppo pine plantation. Ecol.
710 Model. 308, 34–44.

711 Grant, G.E., Tague, C.L., Allen, C.D., 2013. Watering the forest for the trees: an
712 emerging priority for managing water in forest landscapes. Front. Ecol. Environ. 11(6),
713 314–321

714 Grey, D., Sadoff, C.W., 2007. Sink or Swim? Water security for growth and
715 development. Water Policy 9, 545–571.

716 Hibbert, A.R., Davis, E.A., Knipe, O.D., 1982. Water yield changes resulting from
717 treatment of Arizona chaparral. In Dynamics and management of Mediterranean-type
718 ecosystems, tech. coords. C.E. Conrad and W, C. Oechel. USDA For. Serv. Gen. Tech.
719 Rep. PSW-58

720 Hurteau, M.D., Koch, G.W., Hungate, B.A., 2008. Carbon protection and fire risk
721 reduction: toward a full accounting of forest carbon offsets. Front. Ecol. Environ. 6(9),
722 493–498.

723 Ilstedt, U., Bargués-Tobella, A., Bazié, H.R., Bayala, J., Verbeeten, E., Nyberg, G.,
724 Sanou, J., Benegas, L., Murdiyarso, D., Laudon, H., Sheil, D., Malmer, A., 2016.
725 Intermediate tree cover can maximize groundwater recharge in the seasonally dry
726 tropics. Sci. Rep. 6, 21930.

727 Jiang, J., Sharma, A., Sivakumar, B., Wang, P., 2014. A global assessment of climate–
728 water quality relationships in large rivers: An elasticity perspective. Sci. Total Environ.
729 468–469, 877–891.

730 Klein, T., Shpringer, I., Fikler, B., Elbaz, G., Cohen, S., Yakir, Y., 2013. Relationships
731 between stomatal regulation, water-use, and water-use efficiency of two coexisting key
732 Mediterranean tree species. For. Ecol. Manage. 302, 34–42.

733 Liang, W. L., Kosugi, K. I., Mizuyama, T., 2011. Soil water dynamics around a tree on a
734 hillslope with or without rainwater supplied by stemflow. Water Resour. Res. 47(2),
735 W02541. doi:10.1029/2010WR009856.

736 Lin, H., Zhou, X., 2008. Evidence of subsurface preferential flow using soil hydrologic
737 monitoring in the Shale Hills catchment. Eur. J. Soil Sci. 59, 34–49.

738 Lindner, M., Fitzgerald, J.B., Zimmermann, N.E., Reyer, C., Delzon, S., van der
739 Maaten, E., Schelhaas, M.J., Lasch, P., Eggers, J., van der Maaten-Theunissen, M.,
740 Suckow, F., Psomas, A., Poulter, B., Hanewinkel, M., 2014. Climate change and
741 European forests: what do we know, what are the uncertainties, and what are the
742 implications for forest management? J. Environ. Manage. 146, 69-83.

743 Llasat, M.C., 2001. An objective classification of rainfall events on the basis of their
744 convective features: application to rainfall intensity in the northeast of Spain. Int. J.
745 Climatol. 21, 1385–1400.

746 López, B.C., Gracia, C.A., Sabaté, S., Keenan, T., 2009. Assessing the resilience of
747 Mediterranean holm oaks to disturbances using selective thinning. Acta Oecol. 35, 849–
748 854.

749 Merino-Martin, L., Moreno-de Las Heras, M., Pérez-Domingo, S., Espigares, T.,
750 Nicolau, J. M., 2012. Hydrological heterogeneity in Mediterranean reclaimed slopes:
751 runoff and sediment yield at the patch and slope scales along a gradient of overland
752 flow. Hydrology and earth system sciences. 16, 1305-1320.

753 Molina, A., del Campo, A., 2012. The effects of experimental thinning on
754 throughfalland stemflow: a contribution towards hydrology-oriented silviculture in
755 Aleppopine plantations. For. Ecol. Manage. 269, 206–213.

756 Molina, A.J., Latron, J., Rubio, C.M., Gallart, F., Llorens, P., 2014. Spatio-temporal
757 variability of soil water content on the local scale in a Mediterranean mountain area
758 (Vallcebre, North Eastern Spain). How different spatio-temporal scales reflect mean soil
759 water content. J. Hydrol. 516, 182-192.

760 Molina, A. J., Llorens, P., Garcia-Estringana, P., de las Heras, M. M., Cayuela, C.,
761 Gallart, F., Latron, J., 2019. Contributions of throughfall, forest and soil characteristics
762 to near-surface soil water-content variability at the plot scale in a mountainous
763 Mediterranean area. Science of The Total Environment, 647, 1421-1432.

764 Moreno-de las Heras, M., Nicolau, J. M., Merino-Martín, L., Wilcox, B. P., 2010. Plot-
765 scale effects on runoff and erosion along a slope degradation gradient, Water Resour.
766 Res. 46, W04503. doi:10.1029/2009WR007875.

767 Muzylo, A., Llorens, P., Domingo, F., 2012. Rainfall partitioning in a deciduous forest
768 plot in leafed and leafless periods. Ecohydrology 5(6), 759–767.

769 Owor, M., Taylor, R.G., Tindimugaya, C., Mwesigwa, D., 2009. Rainfall intensity and
770 groundwater recharge: empirical evidence from the Upper Nile Basin. Environ. Res.
771 Lett. 4, 035009 (6pp).

772 Pan, Y., Birdsey, R.A., Phillips, O.L., Jackson, R.B., 2013. The Structure, distribution,
773 and biomass of the World's Forests. Annu. Rev. Ecol. Evol. Syst. 44, 593–622.

774 Perry, T. D., Jones, J. A., 2017. Summer streamflow deficits from regenerating Douglas-
775 fir forest in the Pacific Northwest, USA. Ecohydrology, 10 (2). doi: 10.1002/eco.1790

776 RStudio Team, 2015. RStudio: Integrated Development for R. RStudio, Inc., Boston,
777 MA URL http://www.rstudio.com/.

778 Ridgeway, G., 2017. Generalized Boosted Regression Models. https://cran.r
779 project.org/web/packages/gbm/gbm.pdf (last accessed 10.05.18).

780 Rosenbaum, U., Bogena, H. R., Herbst, M., Huisman, J. A., Peterson, T. J., Weuthen, A.,
781 Western, A.W., Vereecken, H., 2012. Seasonal and event dynamics of spatial soil
782 moisture patterns at the small catchment scale. Water Resour. Res. 48, W10544,
783 doi:10.1029/2011WR011518.

784 Sahin, V., Hall, M.J., 1996. The effects of afforestation and deforestation on water
785 yields. J. Hydrol. 178, 293-309.

786 Samouëlian, A., Cousin, I., Tabbagh, A., Bruand, A., Richard, G., 2005. Electrical
787 resistivity survey in soil science: a review. Soil and Tillage research, 83, 173-193.

788 Seidl, R., Spies, T. A., Peterson, D. L., Stephens, S. L., Hicke, J. A., 2016. Searching for
789 resilience: addressing the impacts of changing disturbance regimes on forest ecosystem
790 services. J. Appl. Ecol. 53, 120–129.

791 Taniguchi, M., Tsujimura, M., Tanaka, T., 1996. Significance of stemflow in
792 groundwater recharge. 1: Evaluation of the stemflow contribution to recharge using a
793 mass balance approach, Hydrol. Processes 10(1), 71–80.

794 Troendle, C. A., Wilcox, M. S., Bevenger, G. S., Porth, L. S., 2001. The Coon Creek
795 water yield augmentation project: Implementation of timber harvesting technology to
796 increase streamflow. For. Ecol. Manage. 143, 179-187.

797 Tsiko, C.T., Makurira, H., Gerrits, A.M.J, Savenije, H.H.G., 2012. Measuring forest
798 floor and canopy interception in a savannah ecosystem. Phys. Chem. Earth 47–48, 122–
799 127

800 Ungar, E.D., Rotenberg, E., Raz-Yaseef, N., Cohen, S., Yakir, D., Schiller, G., 2013.
801 Transpiration and annual water balance of Aleppo pine in a semiarid region:
802 implications for forest management. For. Ecol. Manage. 298, 39–51.

803

804 TABLE CAPTIONS

805 **Table 1.** Physiographic, climatic and edaphic features in both experimental sites
806 (Calderona, CAL and Hunde, HU). [a]Fractions in the following order: sand (2–0.02mm),
807 silt (0.02–0.002mm), clay (<0.002 mm). [b] Intervals are for soil depth (cm), with O
808 referring to the superficial organic layer. [c]WHC: water-holding capacity (water content
809 by weight). [e]SOC: soil organic carbon (Walkley–Black). Values are mean±standard
810 deviation.

811 **Table 2.** Means ± standard deviations of forest structure metrics in control (C) and
812 thinned (T) plots for both sites (CAL: Calderona; HU: La Hunde). BA: basal area; D_B:
813 basal diameter; D_{BH}: diameter at breast height; LAI: leaf area index.

814 **Table 3**. Characteristics of the studied rainfall events and meteorological conditions
815 during rainfall in both sites (Calderona, CAL and La Hunde, HU) first classified by
816 convectiveness ($\beta_{L,10}$; $\beta=0$ for non-convective and $\beta\neq0$ for convective events), and second
817 by those causing either drainage, P(D); generalized drainage, P(Dgen); or runoff P(RO).

Pg: gross rainfall, P_D: duration of gross rainfall; P_I: mean rainfall intensity, P_{Imx}: maximum rainfall intensity (10 min); P_{Gap}: time frequency without rainfall in an event, T: air temperature, VPD: water vapor deficit, U_{mx}: maximum wind speed, U_{av}: mean wind speed. Values reports are means; medians (left) and standard deviations (right) in parenthesis (omitted in some variables for simplicity).

Table 4. Cross-validation correlation coefficients obtained in the BRT models fitted for soil water replenishment (Δθ), runoff (RO) and drainage (D, Dgen for generalized drainage) in both sites separately and together (overall). The analyses were performed either on the depth- or the rate-expressed variables. The average and range of the standard error of the coefficients presented are 0.032 and 0.01-0.08 respectively.

FIGURE CAPTIONS

Figure 1. Pictures showing the thinned plots in the studied sites (a, CAL; b, HU) and the trenches for collecting the surface and sub subsurface flows (c, CAL; d, HU). A location map of the studied sites is showed in del Campo et al. (2018).

Figure 2. Three-dimensional representation of the resistivity values (Ohm.m) obtained in the electrical tomography survey in CAL (top) and HU (bottom) sites. Blueish colors correspond to soil (B horizons), green to yellowish to soil with high rock fraction and C horizon and red to purplish to the rock substrate. Units in axes are meters.

Figure 3. Relative importance (RI, %) obtained in the BRT models for the four groups of independent variables (antecedent soil moisture content, θ_{st_rel}; forest structure, FOR_Str; meteorological conditions during rainfall, MET; and rainfall characteristics, RAIN) affecting soil water replenishment (Δθ), runoff (RO), drainage (D, drainage) and generalized drainage (Dgen), in both sites separately and together (overall). The dependent variables were expressed in mm (left) or as % of gross rainfall (right).

Figure 4. Mean and median values in CAL and HU for the antecedent and maximum soil moisture (θ_{mx_rel} and θ_{st_rel}, % of range), soil water replenishment ($\Delta\theta$, mm and % of Pg). C: control, T: thinned plot. Error bars indicate standard deviation of the means. Different letters indicate significant differences between the plots for a site (ANCOVA results are presented in Table 2S as supplemental material).

Figure 5. Mean and median values in CAL and HU for drainage (D, mm and % of Pg), generalized drainage (Dgen, mm and % of Pg) and runoff (RO, mm and % of Pg). C: control, T: thinned plot. Error bars indicate standard deviation of the means. Different letters indicate significant differences between the plots in a site (ANCOVA results are presented in Table 2S as supplemental material).

Figure 6. Temporal dynamics (mm) of runoff (RO), drainage (D) and generalized drainage (Dgen) in the CAL plots. Pg is also represented and those events producing response in each variable are highlighted in red color. The background shaded area indicates the period when the piezometers were monitored, whereas the dark grey bars indicate positive response, with their breadth indicating the period corresponding to a single observation and their height the proportion of piezometers in which the response was detected (%, 4 piezometers for each experimental plot). T: thinned (left); C: control (right).

Figure 7. Temporal dynamics (mm) of runoff (RO), drainage (D) and generalized drainage (Dgen) in the HU plots. Pg is also represented and those events producing response in each variable are highlighted in red color. The background shaded area indicates the period when the piezometers were monitored, whereas the dark grey bars indicate positive response. Height of these dark grey bars indicate the proportion of piezometers in which water was detected (%, 4 piezometers for each experimental plot). Bailer malfunctioning made that only automatic readings during the last year of

868 experiment were available for comparisons. Figure 4S in supplemental material shows
869 examples of automatic readings for two rainfall events. T: thinned (left); C: control
870 (right).

871 **Figure 8.** Cumulative treatment impacts according to site (CAL, HU) on response
872 variables (soil moisture replenishment, $\Delta\theta$; drainage, D; and generalized drainage, Dgen)
873 as a shift in the daily ratio of thinned/control, L (T/C), following the intervention (baseline
874 before thinning treatment is assumed to be zero). Gross rainfall (Pg) is also represented

875 **Figure 9**. Annual water balance (mm) according to site (CAL, HU) and treatment (C, T).
876 Net rainfall (Pn_Thr+Stf) was obtained from del Campo et al. (2018) as the sum of
877 throughfall and stemflow per event. Pg represents gross rainfall, $\Delta\theta$ represents soil
878 moisture replenishment and D represents drainage.

879 **Figure 10**. Elasticity analyses comparing the median values for the experimental plots
880 in the two studied sites (CAL and HU). The ratio [Dgen+RO]/[Pg-Dgen-RO] was
881 considered as a proxy to the blue to green water ratio (b/g), Dgen represents generalized
882 drainage and θ_{mx} is the maximum soil moisture.

883
884 **Table 1.**
885

Site characteristics	Units	CAL	HU
Slope	%	27.8±8.5	32.0±6.0
Aspect	º	311±10 (NW)	319±21 (NW)
P	mm	342	466
T	ºC	14.0	12.8
PET	mm	837	749
Aboveground Biomass (Carbon)	Mg ha^{-1}	47.3 (22.2)	49.7 (23.1)
Texture[a]	%	42.1±7.4;31.4±6.3;26.4±4.0	49.7±6.6;29.3±5.5;20.7±2.1
Stoniness[b]	% vol.	O: 55±25 0-10: 34±21 10-30: 20±19 >30: 5±5	O: 53±8 0-10: 64±8 10-30: 66±17 30-40: 56±5
WHC[c]	%	73±2	122±15
Ks	mm h^{-1}	461	785

SOC[e]	g Kg^{-1}	28.5±22.1	103.5±32.4
pH	(water)	8.3±0.2	7.9±0.2
Carbonates	(g g^{-1}dry soil)	0.34±0.15	0.24±0.10

886

887

888 **Table 2.**

Plot	**D_B** (cm)	**D_{BH}** (cm)	**BA** (m^2 ha^{-1})	**Density** (tree ha^{-1})	**Cover** (%)	**LAI** (m^2 m^{-2})
CAL-C	4.60±3.65	2.92±2.52	18.6±4.6	12280±12202	78.7±14.0	1.5±0.2
CAL-T	13.18±4.2	8.51±3.12	4.5±0.8	703±232	38.7±11.5	0.5±0.1
HU-C	11.87±0.25	8.5±0.5	8.2±3.8	1112±308	62.7±2.3	1.1±0.2
HU-T	16.7±2.2	12.9±1.8	5.0±1.2	306±34	39.3±4.2	0.6±0.1

889

890

891 **Table 3.**

Gross Rainfall types	**N**	**Pg** (mm)	**P_D** (min)	**P_I** (mm h^{-1})	**P_{Imx}** (mm h^{-1}, Δt=10 min)	**P_{Gap}** (% time)	**$\beta_{L,10}$**	**T** (°C)	**VPD** (Pa)	**U_{mx}** (m s^{-1})	**U_{av}** (m s^{-1})
CALDERONA (CAL)											
Pg (non-convective)	106	4.0 (2.6;3.9)	128 (91;118)	2.9 (2.1;3.2)	5.9 (4.8;4.7)	45	0	9.6	138	6.6	2.3
Pg (convective)	10	26.2 (19.7;24.4)	171 (95;190)	12.4 (7.4;8.6)	40.4 (40.8;11.5)	20	0.50	13.3	247	10.9	3.7
P_D	41	11.6 (7.2;15.1)	182 (125;165)	5.1 (3.0;6.0)	16.6 (10.4;15.7)	39	0.121	9.7	112	7.8	2.5
P_{Dgen}	32	12.9 (7.7;16.7)	184 (134;160)	5.2 (3.7;5.9)	18.2 (12;16.1)	41	0.127	9.9	106	7.3	2.2
P_{RO}	25	16.3 (11.6;17.6)	236 (178;184)	5.7 (3.7;6.5)	20.8 (16.8;16.6)	38	0.149	9.2	74	8.4	2.6
LA HUNDE (HU)											
Pg (non-convective)	226	5.0 (2.8;6.2)	240 (150;303)	1.7 (1.2;1.7)	4.1 (2.9;3.7)	40	0	8.1	127	3.5	0.7
Pg (convective)	10	13.4 (12.4;8.0)	98 (83;73)	11.3 (9.8;7.0)	34.3 (31.5;11.1)	40	0.61	16.2	186	3.4	0.5
P_D	146	6.5 (3.6;7.2)	280 (180;347)	2.1 (1.3;2.9)	5.7 (3.2;7.9)	23	0.030	7.4	74	4.3	0.9
P_{Dgen}	118	7.4 (4.0;7.7)	321 (205;374)	2 (1.3;2.8)	5.7 (3.6;7.9)	27	0.022	7.2	66	4.3	0.9
P_{RO}	149	6.6 (4.0;7.0)	264 (170;343)	2.5 (1.4;3.4)	6.6 (3.6;8.8)	21	0.041	8.7	106	4.2	0.8

892

893 **Table 4.**

Hydrological Variable	**CAL**	**HU**	**OVERALL**

Depth (mm)	**Δθ**	0.873	0.823	0.877
	D	0.956	0.929	0.923
	Dgen	0.918	0.853	0.875
	RO	0.921	0.572	0.864
Rate (%Pg)	**Δθ**	0.783	0.726	0.765
	D	0.902	0.805	0.833
	D gen	0.820	0.700	0.734
	RO	0.800	0.577	0.734

894

894

895 **Figure 1**

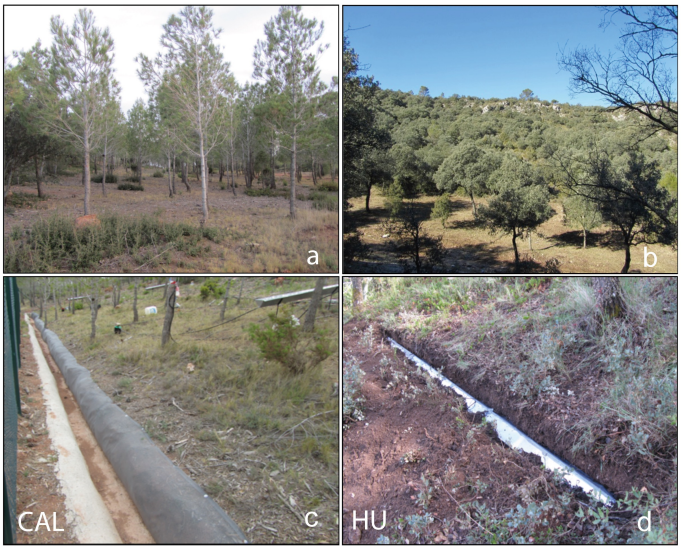

896

897 **Figure 2**

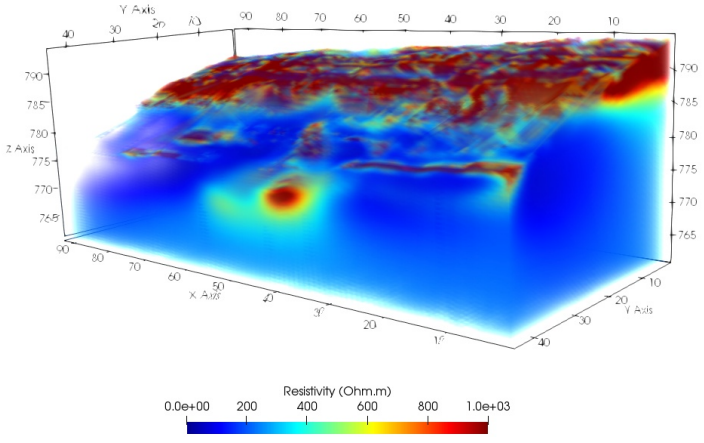

898

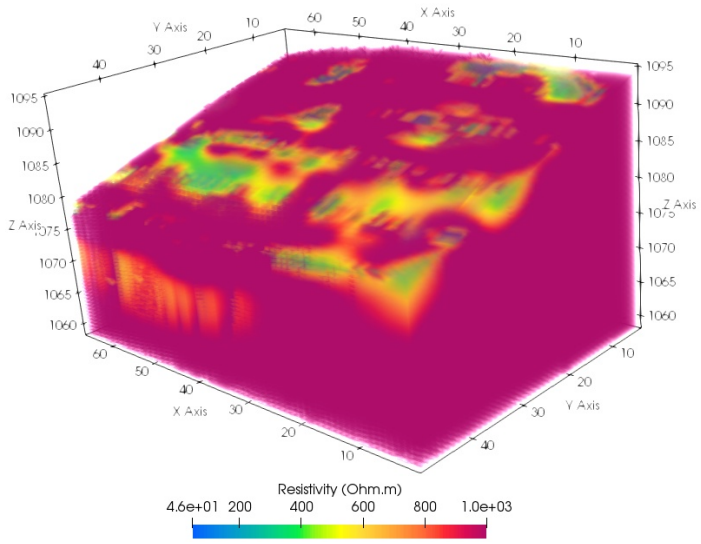

899

900 **Figure 3**

901

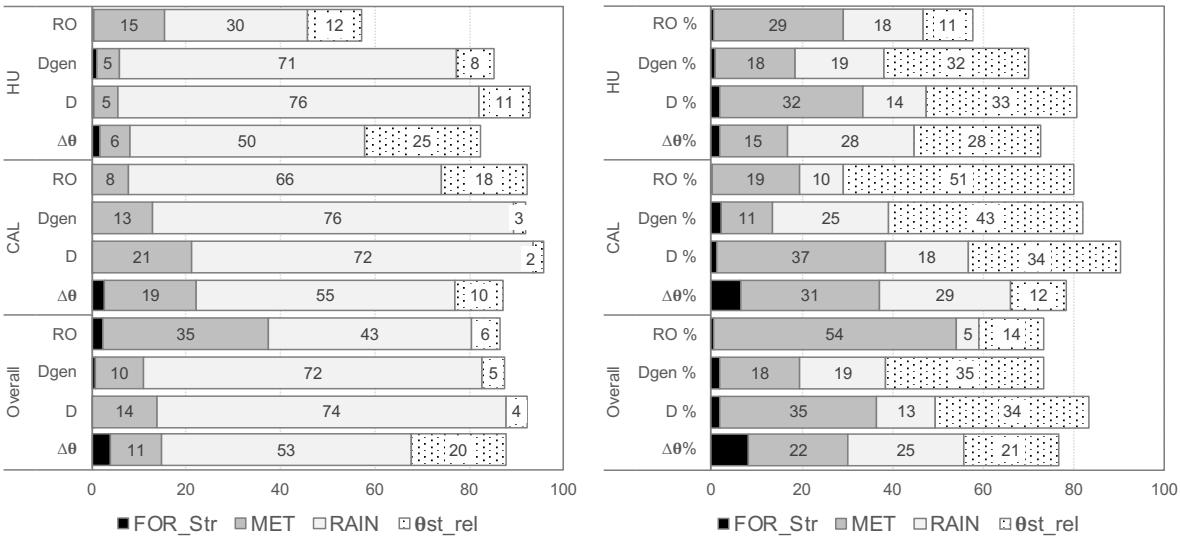

902

903 **Figure 4**

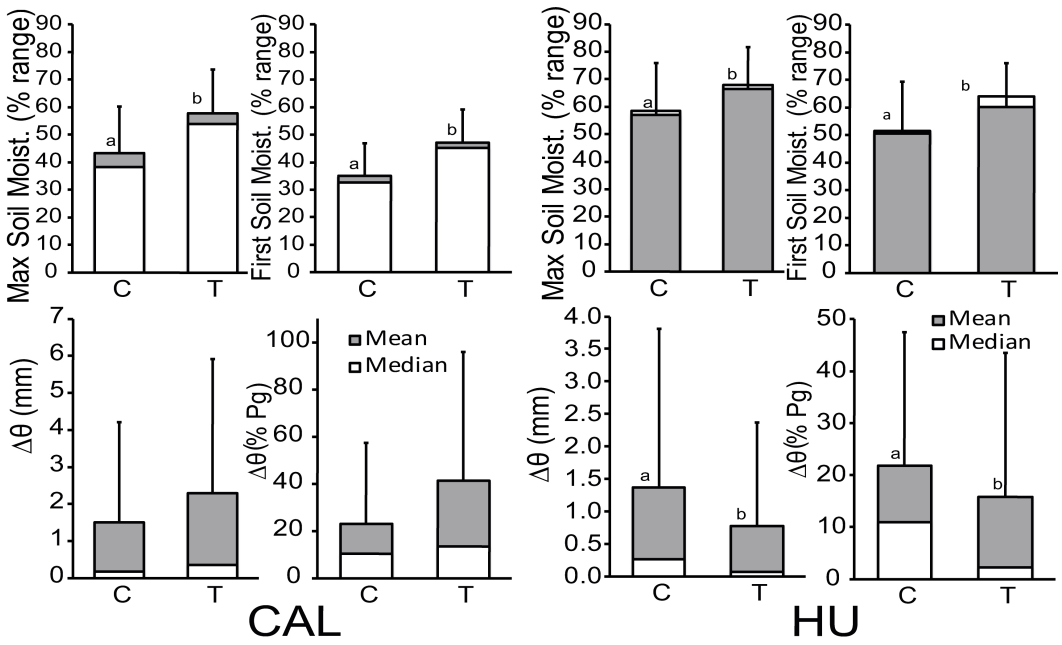

904

905 **Figure 5**

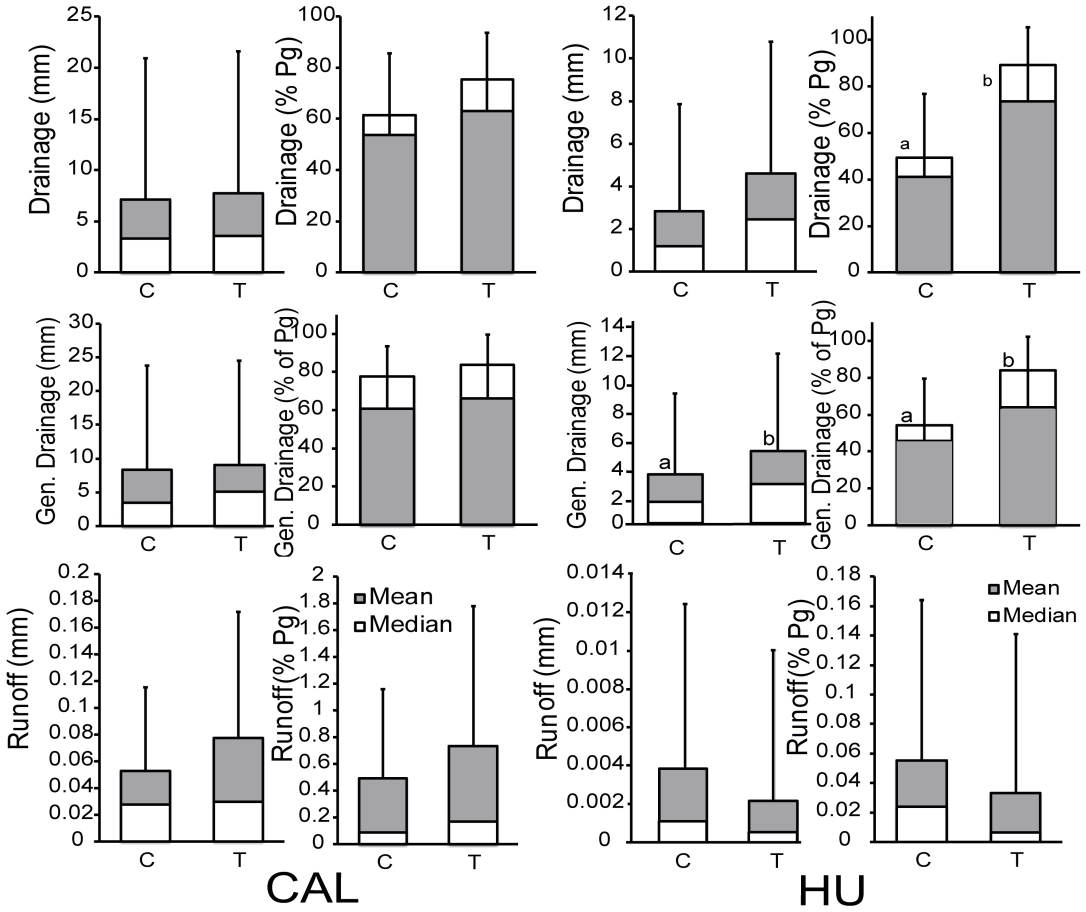

906

907 **Figure 6**

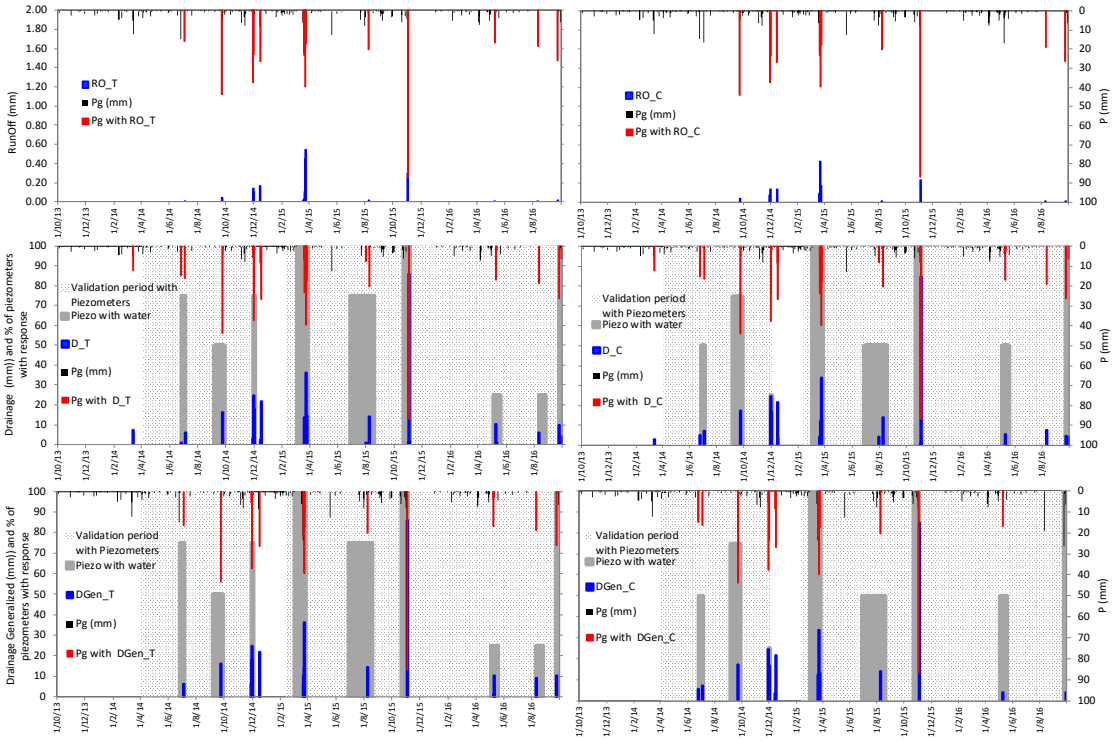

908

909 **Figure 7**

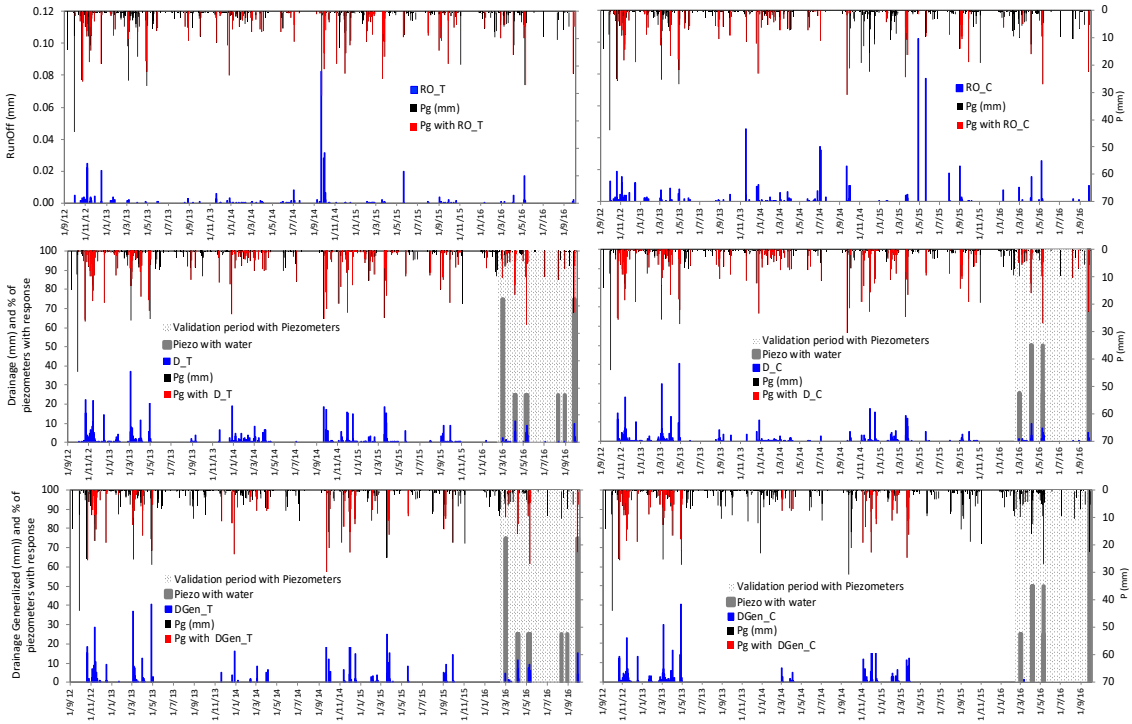

910

911 **Figure 8**

912

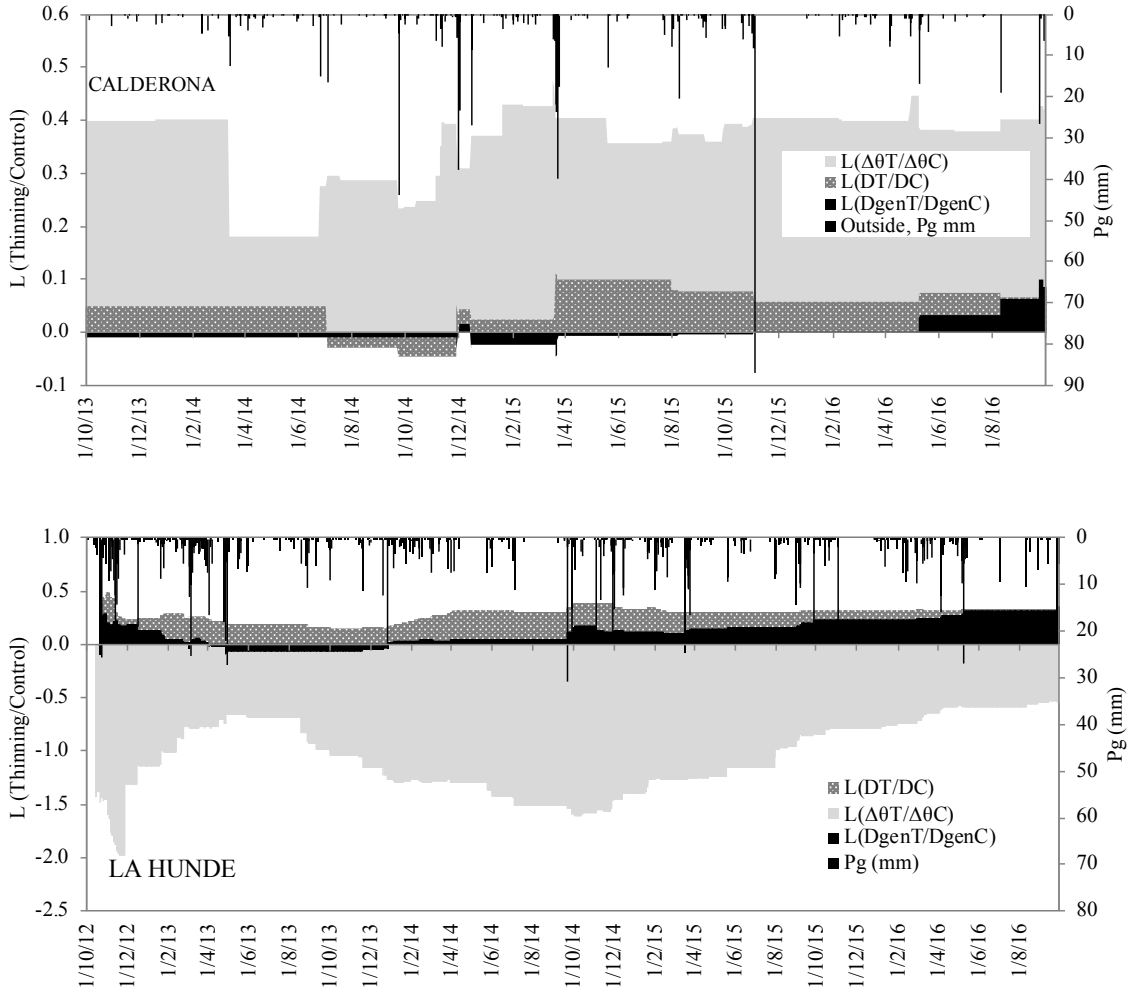

913

914 **Figure 9**

915

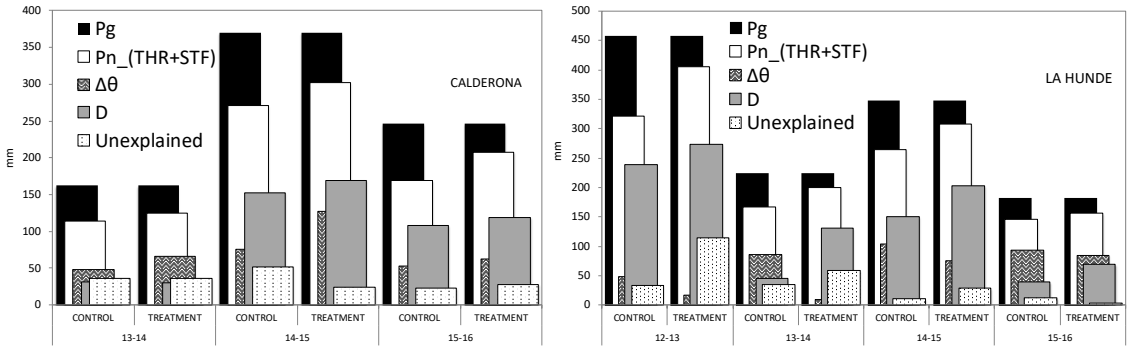

916

917 **Figure 10**

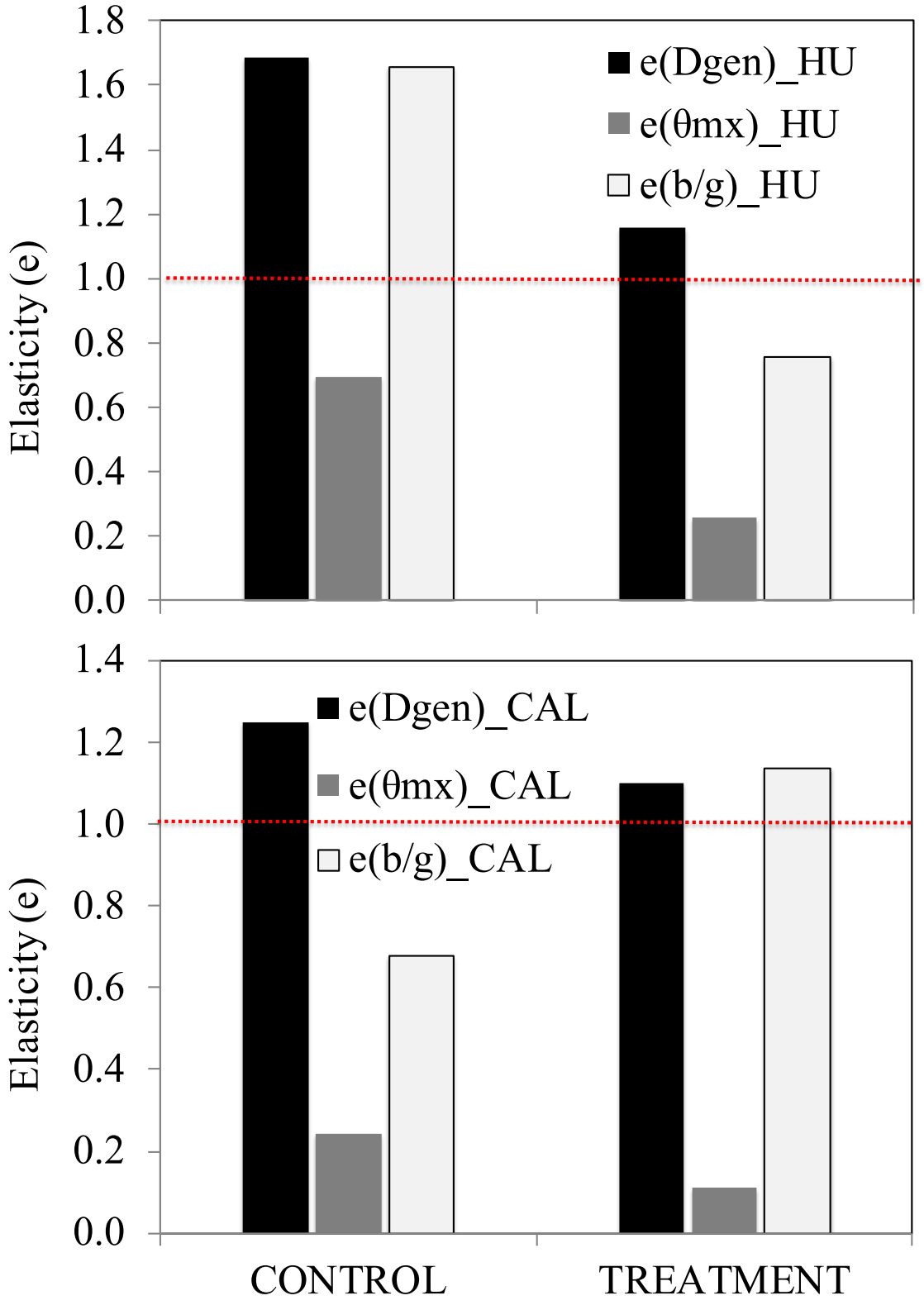
1.8
1.6
1.4
1.2
1.0
0.8
0.6
0.4
0.2
0.0
Elasticity (e)
e(Dgen)_HU
e(θmx)_HU
e(b/g)_HU
1.4
1.2
1.0
0.8
0.6
0.4
0.2
0.0
Elasticity (e)
e(Dgen)_CAL
e(θmx)_CAL
e(b/g)_CAL
CONTROL
TREATMENT